

Accidental Double Dirac Cones and Robust Edge States in Topological Anisotropic Photonic Crystals

Xiao-Dong Chen, Wei-Min Deng, Fu-Li Zhao, and Jian-Wen Dong*

Dirac cones in photonic systems have many profound applications such as achieving zero-index materials and nontrivial photonic phases. It is shown that double Dirac cones at the zone boundary can be restored by achieving accidental degeneracy between transverse electric and transverse magnetic modes in 2D photonic crystals with anisotropic permittivity. The topological band gap can be obtained by lifting nontrivial double Dirac cones, each of which is formed by two orthogonally polarized linear branches sharing the same mirror parities. Robust transport of gapless and high transmission of gapped edge states are also demonstrated in topological anisotropic photonic crystals, demonstrating that a high transmission flat-top spectrum is observed in various working frequency regions even when the interface is no longer straight. This may pave the way to a paradigm for a bandwidth-controllable robust waveguide in topological photonics.

1. Introduction

Conical dispersions, such as Dirac cones^[1–3] and Weyl points,^[4–7] have been widely studied in various fields due to the analogies between different solid state systems. For example, photonic crystals (PCs) with a single Dirac cone at Brillouin zone center behave as zero-index metamaterials at a finite frequency,^[8,9] leading to the realization of invisibility cloak,^[10] asymmetric transmission,^[11] and directional emission.^[12,13] On the other hand, topological phases characterized by nonzero Berry curvature in momentum space can be obtained by breaking single or double Dirac cones at zone center^[14–17] or zone boundary.^[18–23] It provides a new degree of freedom to control the flow of electron, sound or light, leading to some novel phenomena such as spin-direction locking edge states and robust transport immune to defects.^[2,3,24–30] With regard to the time-reversal invariant photonic systems, one key point for the realization of topological PCs with nonzero spin Chern number is to construct double Dirac cones. One representative method is to introduce the electromagnetic (EM) duality symmetry, that is, $\varepsilon = \mu$.^[20,31] However, the magnetic response is inherently weak at optical frequencies, and

the EM duality symmetry will be broken in non-magnetic systems. As a result, double Dirac cones cannot be guaranteed and how can we restore the double Dirac cones in non-magnetic systems? On the other hand, the topologically protected edge states exhibit gapless feature if the obstacles do not violate topological protection. While in realistic photonic systems, the gapless feature is not always guaranteed and gapped photonic edge states show up. Then another question arises: can the robust transport or high transmission against obstacles be preserved for the gapped edge states in topological band gaps?


In this work, we show that double Dirac cones at zone boundary can be restored in PCs with anisotropic permittivity by achieving accidental degeneracy between transverse electric (TE) and transverse magnetic (TM) modes. Under nonzero bianisotropy, we generalize the band gap opening condition by exploiting the degenerate perturbation theory and mode symmetry analysis. We demonstrate that the realization of double Dirac cones is not the sufficient condition to open the band gap, and we should consider the parity of TE and TM modes. Nontrivial double Dirac cones, each of which consists of TE and TM modes sharing the same mirror parity, transform into a topological band gap. We construct such nontrivial double Dirac cones by the anisotropic permittivity configuration and obtain topological anisotropic PCs. Gapless edge states and their robustness against bends with different turning angles are demonstrated at the domain wall between two topologically distinct anisotropic PCs. Last, we present the high transmission of gapped edge states in the topological anisotropic PC, showing as a comparison to the strongly backscattered gapped edge states in the trivial PC.

2. Results and Discussion

2.1. Accidental Double Dirac Cones

To have Dirac cones at the zone boundary, let us consider a 2D triangular PC (**Figure 1a**). It consists of periodic circular rods (labeled as region 2) embedded in background (labeled as region 1). We choose the radius of rods to be $r = 0.407a$ where a is the lattice constant. As the EM duality symmetry is broken in non-magnetic systems, TE- and TM-polarized Dirac cones near zone boundary (i.e., K point) have different frequencies.

Dr. X.-D. Chen, W.-M. Deng, Prof. F.-L. Zhao, Prof. J.-W. Dong
School of Physics and State Key Laboratory of Optoelectronic Materials and Technologies
Sun Yat-sen University
Guangzhou 510275, China
E-mail: dongjwen@mail.sysu.edu.cn

 The ORCID identification number(s) for the author(s) of this article can be found under <https://doi.org/10.1002/lpor.201800073>

DOI: 10.1002/lpor.201800073

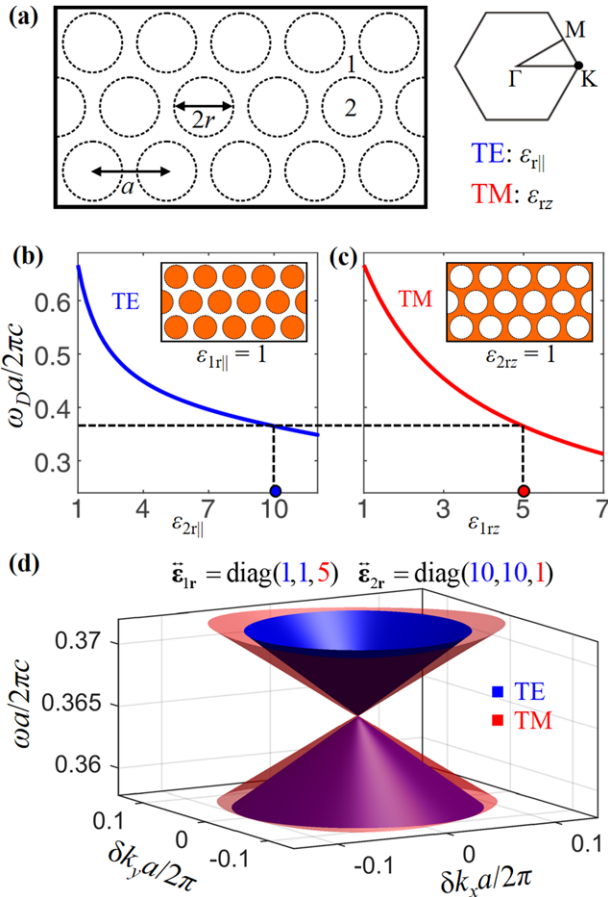


Figure 1. Accidental double Dirac cones in anisotropic photonic crystals (PCs). a) Schematic of triangular PC consisting of circular rods (labeled by region 2) in background (labeled by region 1). The radii of rods are set to be $r = 0.407a$ where a is the lattice constant. The right inset shows the first Brillouin zone with high symmetry k -points. The frequencies of TE and TM modes are respectively tuned by the in-plane ($\varepsilon_{||}$) and out-of-plane (ε_{\perp}) component of permittivity in non-magnetic systems. b) Evolution of Dirac frequency of the lowest TE dipolar mode at K point along the in-plane permittivity of region 2 ($\varepsilon_{2||}$). Orange color (Inset) shows that region 2 of PC is filled with high ε medium for TE polarization. c) Similar to (b) but evolution of Dirac frequency of the lowest TM dipolar mode along the in-plane permittivity of region 1 ($\varepsilon_{1\perp}$). In contrast to materials configuration in (b), orange color (Inset) shows that region 1 of PC is filled with high ε medium for TM polarization. d) 3D eigen-frequency surfaces for TE (blue) and TM (red) polarizations showing the accidental double Dirac cones in anisotropic PC with $\vec{\varepsilon}_{1r} = \text{diag}(1, 1, 5)$ and $\vec{\varepsilon}_{2r} = \text{diag}(10, 10, 1)$.

However, because TE and TM polarized dispersions are separately determined by the in-plane and out-of-plane component of permittivity, we can restore the accidental double Dirac cones by tuning the anisotropic permittivity. To see this, we fix $\varepsilon_{1||} = 1$ at region 1 while fill region 2 with high ε medium (orange rods) for the TE polarization (inset of Figure 1b). Figure 1b plots the evolution of the Dirac frequency of the lowest TE dipolar states at K point as a function of the in-plane permittivity of region 2 ($\varepsilon_{2||}$). With the increasing of $\varepsilon_{2||}$, the TE Dirac frequency decreases monotonously. In contrast, for TM polarization, we fill region 1 with high ε medium (orange background) while fix $\varepsilon_{2\perp} = 1$ at region 2 (inset of Figure 1c). Figure 1c shows that the

Dirac frequency of TM dipolar modes decreases monotonously with the increasing of the out-of-plane permittivity of region 1 ($\varepsilon_{1\perp}$). We fix one frequency (e.g., $f = 0.365c/a$) and draw a horizontal dashed black line. It intersects with the TE (TM) dipolar mode dispersion at $\varepsilon_{2||} = 10$ ($\varepsilon_{1\perp} = 5$). It tells us that when regions 1 and 2 are respectively filled with anisotropic medium of $\vec{\varepsilon}_{1r} = \text{diag}(1, 1, 5)$ and $\vec{\varepsilon}_{2r} = \text{diag}(10, 10, 1)$, accidental double Dirac cones can be restored. Figure 1d shows the 3D eigen-frequency surface near K point. The conical dispersions for TE (blue) and TM (red) polarizations are found and they are accidentally degenerate at $f = 0.365c/a$, proving the realization of accidental double Dirac cones in anisotropic PCs.

2.2. Band Gap Opening Condition

Before presenting topological anisotropic PCs by breaking the accidental double Dirac cones, we analyze the band gap opening condition. Consider a 2D anisotropic PC under nonzero bianisotropy, the constitutive relations are $\vec{D} = \varepsilon_0 \vec{\varepsilon}_r \vec{E} + \vec{\zeta} \vec{H}$ and $\vec{B} = \mu_0 \vec{\mu}_r \vec{H} + \vec{\zeta} \vec{E}$. Here, $\vec{\varepsilon}_r = \text{diag}(\varepsilon_{||}, \varepsilon_{||}, \varepsilon_{\perp})$ is the anisotropic permittivity and $\vec{\mu}_r = 1$ is the permeability. $\vec{\zeta}$ is the bianisotropic tensor with nonzero elements of $\zeta_{12} = \zeta_{21}^* = i\zeta_0/c$ in which ζ_0 characterize the coupling strength between TE and TM modes. The Maxwell equations can be written in the matrix form:

$$\begin{pmatrix} i\tilde{\zeta} & i\tilde{n} \\ \tilde{n}^2 - \tilde{\zeta}^2 & \tilde{n}^2 - \tilde{\zeta}^2 \end{pmatrix} \begin{pmatrix} \nabla \times \vec{E} \\ \nabla \times \vec{H} \end{pmatrix} = \tilde{\omega} \begin{pmatrix} \vec{E} \\ \vec{H} \end{pmatrix} \quad (1)$$

where the normalized quantities are $\vec{E} = \sqrt{\varepsilon_0 \vec{\varepsilon}_r} \vec{E}$, $\vec{H} = \sqrt{\mu_0} \vec{H}$, $\tilde{n} = \sqrt{\vec{\varepsilon}_r \vec{\mu}_r} = \sqrt{\vec{\varepsilon}_r}$, $\tilde{\omega} = \omega/c$, and $\tilde{\zeta} = \vec{\zeta} c$ with c is the velocity of light in vacuum. When $\zeta_0 = 0$, TE and TM modes are decoupled. In general, the dispersion bands of these two polarizations differ and cross to each other. In the presence of nonzero bianisotropy, eigen-fields of TE and TM modes will couple and the evolution of dispersion bands can be analyzed by the degenerate perturbation theory.^[32] Here, we have the unperturbed Hamiltonian for $\zeta_0 = 0$ (H_0) and the perturbed Hamiltonian upon nonzero bianisotropy ($H_0 + \Delta H$):

$$H_0 = \begin{pmatrix} 0 & \frac{i}{\tilde{n}} \nabla \times \\ -\frac{i}{\tilde{n}} \nabla \times & 0 \end{pmatrix}, \quad \Delta H = \begin{pmatrix} \frac{i\tilde{\zeta}}{\tilde{n}^2 - \tilde{\zeta}^2} \nabla \times & \frac{i\tilde{\zeta}^2}{\tilde{n}^3} \nabla \times \\ -\frac{i\tilde{\zeta}^2}{\tilde{n}^3} \nabla \times & \frac{-i\tilde{\zeta}}{\tilde{n}^2 - \tilde{\zeta}^2} \nabla \times \end{pmatrix} \quad (2)$$

We suppose that the eigen-solutions of H_0 and $H_0 + \Delta H$ are (\vec{E}_m, \vec{H}_m) and (E', H') with $E' = \sum_m a_m \vec{E}_m$, $H' = \sum_m a_m \vec{H}_m$, and a_m is the hybridized coefficient with m running from TE to TM. The secular equation for the perturbed eigen-frequency ω' is

$$\begin{pmatrix} \omega_{TE} + \Delta H_{TE,TE} & \Delta H_{TE,TM} \\ \Delta H_{TM,TE} & \omega_{TM} + \Delta H_{TM,TM} \end{pmatrix} \begin{pmatrix} a_{TE} \\ a_{TM} \end{pmatrix} = \omega' \begin{pmatrix} a_{TE} \\ a_{TM} \end{pmatrix} \quad (3)$$

Here, $\Delta H_{m,n} = \langle (\tilde{E}_m, \tilde{H}_m) | \Delta H | (\tilde{E}_n, \tilde{H}_n) \rangle$ is integrated inside the unit cell of PC. After the block diagonalization of Equation (3), the perturbed eigen-frequency can be expressed as

$$\omega'_{\pm} = \omega_D + (\Delta H_{TE,TE} + \Delta H_{TM,TM} - v_{TE}\delta k + v_{TM}\delta k) / 2 \pm \sqrt{(-\Delta H_{TE,TE} + \Delta H_{TM,TM} + v_{TE}\delta k + v_{TM}\delta k)^2 / 2 + \Delta H_{TE,TM} \cdot \Delta H_{TM,TE}} \quad (4)$$

Here, the frequency dispersions of coupled TE and TM modes are assumed to be $\omega_{TE} = \omega_D - v_{TE}\delta k$ and $\omega_{TM} = \omega_D + v_{TM}\delta k$, with δk being the distance between wave vector of \vec{k} and wave vector of crossing k -point of TE and TM dispersions. If $\Delta H_{TE,TM} \cdot \Delta H_{TM,TE} = 0$, the square root in Equation (4) reduces into a linear function of δk . Then $\omega'_+ = \omega'_-$ will always be satisfied at one δk , and the band gap fails to open. So the generalized band gap opening condition under nonzero bianisotropy is $\Delta H_{TE,TM} \cdot \Delta H_{TM,TE} \neq 0$. Although the calculation of $\Delta H_{m,n}$ is a bit tedious due to the complexity of the integration, we just need to determine whether $\Delta H_{m,n}$ is nonzero or not. In this regard, mode symmetry analysis is a simple way to solve this problem.^[33] For triangular PCs, $\Delta H_{m,n} \neq 0$ is equivalent to that the irreducible representations of TE and TM modes under mirror operation are the same, that is, $\sigma(TE) = \sigma(TM)$. The detailed discussion of the band gap opening condition with mode symmetry analysis is given in Supporting Information A.

2.3. Topological Band Gap

Considering the group symmetries of interacted TE and TM modes, there are two ways to form accidental double Dirac cones in triangular anisotropic PCs (Figure 2a,d). The first kind of double Dirac cones can be divided into two cones, each of which is formed by TE and TM modes having different parities (Figure 2a). It leads to $\Delta H_{m,n} = 0$ and consequently two cones are only frequency shifted apart and no band gap can be obtained. As an example, we consider the anisotropic PC whose region 1 and 2 are respectively filled with $\vec{\epsilon}_{1r} = \text{diag}(1, 1, 33.55)$ and $\vec{\epsilon}_{2r} = \text{diag}(20, 20, 6.71)$. Such anisotropic PC has a normal double Dirac cones around the frequency of $0.3c/a$ (Figure 2b). These double Dirac cones will not be gapped when nonzero bianisotropy is introduced (Figure 2c). Hence the realization of double Dirac cones is *not* a sufficient condition to have band gaps.

In contrast, as shown in Figure 2d, nontrivial double Dirac cones are constructed by two cones with TE and TM modes sharing the same mirror parity (Figure 2d). So $\Delta H_{m,n} \neq 0$ and a band gap will be obtained after introducing nonzero ζ_0 . As an example of demonstrating the nontrivial double Dirac cones and the resultant topological band gap under nonzero bianisotropy, Figure 2e shows the TE (blue) and TM (red) band structures of the anisotropic PC presented in Figure 1d. After analyzing the mode symmetry of double Dirac cones around the frequency of $0.365c/a$, it is found that these double Dirac cones are nontrivial as each of them is formed by two branches with the same mirror parity. Inferring from the band evolution schematic of Figure 2d, it can be predicted that a band gap will open when a nonzero bianisotropy is applied. A larger bianisotropy results in the band gap with a wider gap bandwidth, for example, a representative

example is plotted in Figure 2f when $\zeta_0 = 0.9$. Around K point, the band dispersion and its evolution under nonzero bianisotropy can be described by $\hat{H} = v_D(\hat{t}_z\hat{s}_0\hat{\sigma}_x\delta k_x + \hat{t}_0\hat{s}_0\hat{\sigma}_y\delta k_y) + \eta\zeta_0\hat{t}_z\hat{s}_z\hat{\sigma}_z$,

where \hat{t}_i , \hat{s}_i , and $\hat{\sigma}_i$ are the Pauli matrices acting on valley, spin, and orbital subspaces. v_D is the group velocity near the Dirac point. $\eta\zeta_0$ ($|2\eta\zeta_0|$ determines the frequency width of band gap opening at K point) is the effective mass induced by the nonzero bianisotropy. η is the gap opening coefficient which can be extracted from the bianisotropy dependent band gap at K point. The

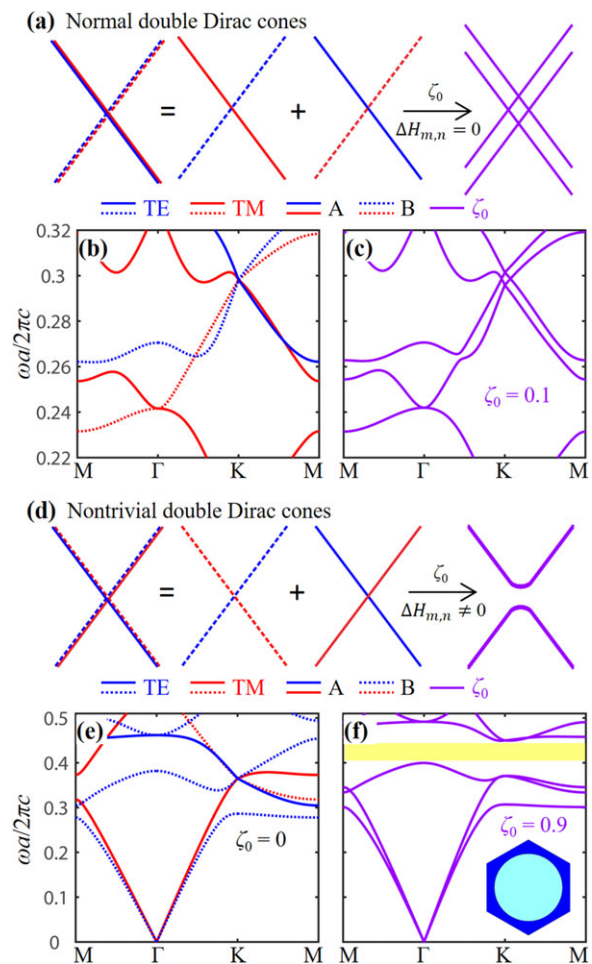


Figure 2. Normal and nontrivial double Dirac cones. a) Schematic of normal double Dirac cones, each of which is formed by TE and TM modes sharing different mirror parities. These double cones are just frequency shifted apart and no band gap is observed when nonzero bianisotropy is applied. b) Normal double Dirac cones and c) Frequency shifted cones in anisotropic PC. d) Schematic of nontrivial double Dirac cones, each of which is formed by TE and TM modes with the same mirror parity. A topological band gap is then obtained under nonzero bianisotropy. e) Nontrivial double Dirac cones in anisotropic PC which have been presented in Figure 1d, around the frequency of $0.365c/a$. f) A topological band gap ranges from $0.4c/a$ to $0.45c/a$ (yellow) when $\zeta_0 = 0.9$. Inset in (f) shows the schematic of the unit cell.

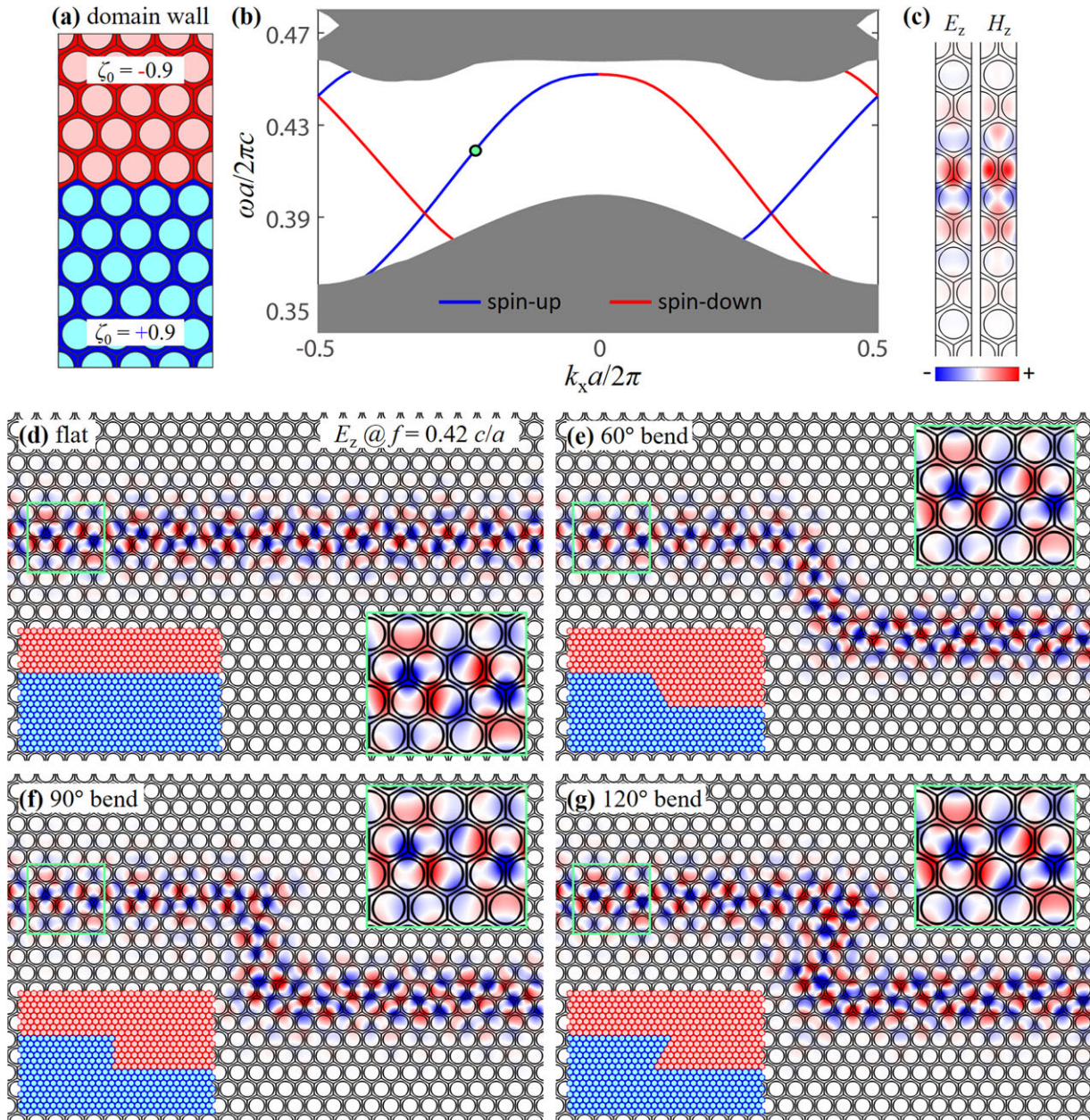


Figure 3. Dispersion bands and robust transport of gapless edge states in the topological anisotropic PC. a) Schematic of the domain wall between two topologically distinct non-magnetic PCs. The top one is applied under $\zeta_0 = -0.9$ while the bottom one is $\zeta_0 = +0.9$. b) Band structures of edge states in which the spin-up and spin-down modes are marked by blue and red curves, respectively. Two gapless edge states dispersions for both spin polarizations are found as the spin Chern number difference across the domain wall is 2. c) Eigen-fields (E_z and H_z) of a representative spin-up mode (marked by a green dot in (b)) at $f = 0.42c/a$ are shown. d–g) Transmissions of edge state with the frequency of $f = 0.42c/a$ when the source is excited at the left end. E_z fields of four kinds of waveguides, that is, d) flat channel, e) 60° bend, f) 90° bend, and g) 120° bend are shown. Schematic of each waveguide is attached at the left-bottom corner. In addition, the zoom-in fields near the entrance are also given. No backscattered waves are observed in (e)–(g) as their zoom-in fields are the same as that in (d), verifying the presence of robust transport of edge states.

detailed derivation of the effective Hamiltonian is presented in Supporting Information B. The bianisotropy (ζ_0) acts on photon in a similar way as the spin-orbital coupling on electron,^[20] and the result spin Chern number of bulk band below the band gap is given by $C_s = \text{sgn}(\eta\zeta_0)$. In this anisotropic PC, $\eta > 0$, and the gap spin Chern number of band gap presented in Figure 2f is $C_{s\text{-gap}} = +1$.

2.4. Robust Edge States

One major interest in topological phases is that they have robust edge states against defects. To see this, we first consider the domain wall which is constructed by two topologically distinct anisotropic PCs (Figure 3a). The lower PC is that presented in Figure 2f with $\zeta_0 = 0.9$ while the upper PC has $\zeta_0 = -0.9$.

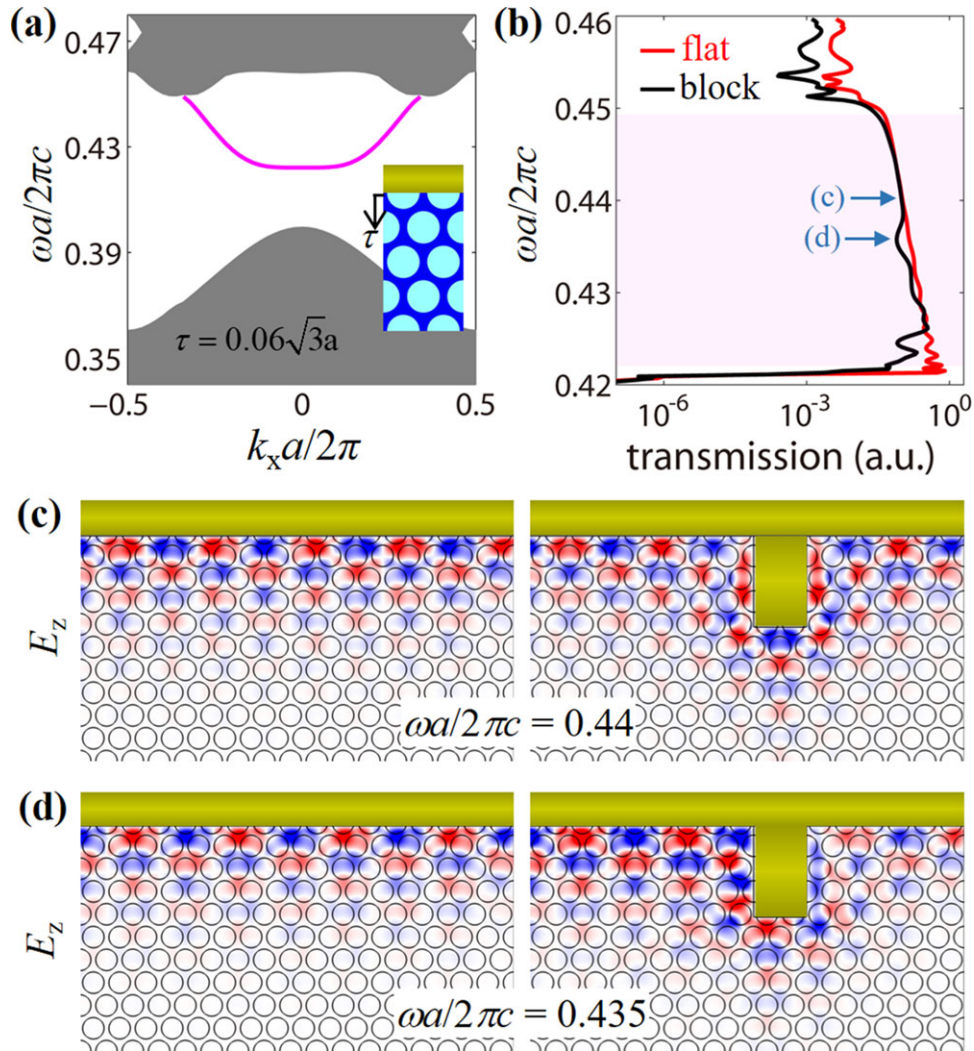


Figure 4. Robust transport and high transmission of gapped edge states in the topological anisotropic PC. a) Gapped edge dispersion (pink) along with projected passing bands (shaded in grey) for the photonic boundary between the topological anisotropic PC and a trivial insulator. The termination of boundary is $\tau = 0.06\sqrt{3}a$, where τ measures the distance from boundary to the center of the outmost rods [inset]. b) Transmission through the flat waveguide (red) and the waveguide with an inserting block (black). At most frequencies (e.g., $f = 0.44c/a$), the transmission of block waveguide is the same as that of flat waveguide. At some frequencies (e.g., $f = 0.435c/a$), the transmission drops little but still keeps high value. c) E_z fields near the blocked boundary at the frequency of $0.44c/a$, showing almost all the EM wave is transmitted. d) E_z fields at the frequency of $0.435c/a$, showing partial transmission of EM waves around the inserting block.

As the spin Chern number difference across the domain wall is 2, there will be two gapless edge state dispersions. This is confirmed by the calculated band structures shown in Figure 3b, in which spin-up and spin-down modes are respectively marked in blue and red. Here, spin-up (spin-down) modes is referred to the eigen-states with in-phase (out-of-phase) E_z and H_z .^[20] For example, Figure 3c shows the eigen-fields of one spin-up state at the frequency of $0.42c/a$ (marked by a green dot in Figure 3b). Both E_z and H_z are localized near and decay away from the domain wall. The phase difference between E_z and H_z is 0, indicating the spin-up polarization. In addition, spin-up modes have positive group velocities while the spin-down modes have negative group velocities inside the band gap. These counter-propagating modes are decoupled to each other^[34,35] and hence robust transport happens. As edge states are protected by the electromagnetic dual

symmetry, they are robust against disorders, such as perturbation of rod position and different bend degree of domain wall. Other defects, for example, an inclusion of perfect electric conductor at the boundary of domain wall will destroy the robust transport behavior. To demonstrate the robustness of gapless edge states, we launch the input source at the left of the domain wall. The rightward propagating EM waves are excited (Figure 3d). Even when they encounter the 60° bend (Figure 3e), 90° bend (Figure 3f), and 120° bend (Figure 3g), the rightward EM waves can go around these defects and keep moving rightward. The ratios of the transmission of 60° bend, 90° bend, and 120° bend to that of the flat waveguide are 0.96, 0.96, and 0.99, respectively. In the simulation, the ratios are a bit different to 1 due to the finite size of numerical calculation. Here, the 90° bend in Figure 3f does not flip the spin as the spin classification is still valid for domain

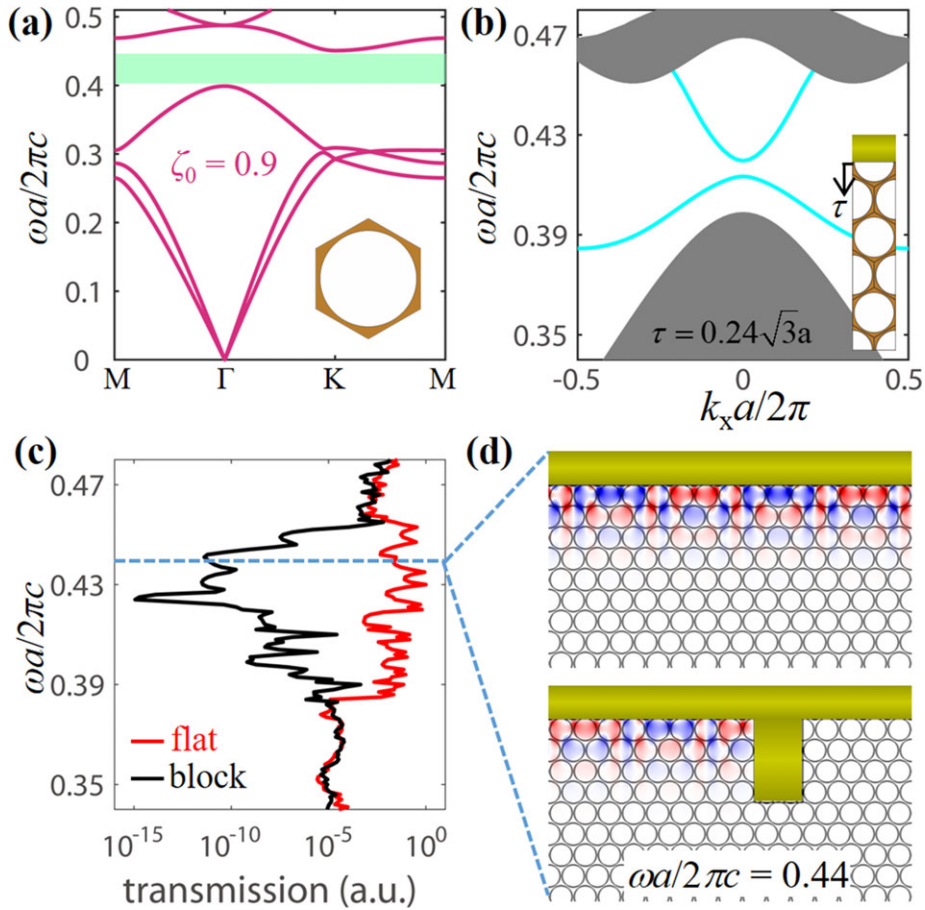


Figure 5. Band structure and transmission for gapped edge states in a trivial PC. a) Band structures of the trivial PC whose unit cell consists of an air hole with $r = 0.46$ embedded in the background with $\epsilon_r = 15$. The bianisotropic coefficient is $\zeta_0 = 0.9$. The band gap (shaded in green) is topologically trivial as no band inversion is observed when ζ_0 increases from 0 to 0.9. b) Gapped dispersion bands of edge states (cyan) within the trivial gap when the photonic boundary termination is $\tau = 0.24\sqrt{3}a$. c) Transmission through the blocked waveguide (black) is several orders of magnitude less than that of the flat waveguide without defect (red), illustrating the wave blocking behavior. d) E_z fields of EM waves at the frequency of $0.44c/a$ show the strong backscattering and zero transmission in the waveguide with an inserting block.

wall with armchair morphology (Supporting Information C). In addition, the zoom-in field patterns in the entrance (outlined by green rectangles in Figure 3d–g) are the same, also proving that there are no backscattered waves when the EM waves meet the bends.

Edge states will not always be gapless and will become gapped at some boundaries. It is questioned whether robust transport or high transmission of gapped edge states can be achieved under the topological protection. To answer this question, we consider a photonic boundary as shown in the inset of Figure 4a. It is constructed between the above-mentioned topological anisotropic PC and a trivial homogeneous insulator that does not allow any EM energy to enter.^[36] To prevent the propagation of EM waves with both two polarizations, the perfect electromagnetic conductors (PEMCs) should be considered.^[37,38] In our simulation, we set the constitutive parameters of this trivial homogeneous insulators as $\epsilon_r = \mu_r = \text{diag}(1, 1, -10\ 000)$ to simplify the calculation. Here, we define the parameter τ ($0 \leq \tau < 0.5\sqrt{3}a$) to indicate the boundary termination position along the ΓM direction of the triangular PC. The boundary locates at the center of the outmost row rods when $\tau = 0$. By continuously altering the boundary

morphology from $\tau = 0$, the spin-up and spin-down edge states move closer and then merge together. As a result, the edge dispersions change to be gapped. For example, the dispersion bands of edge states of the photonic boundary with $\tau = 0.06\sqrt{3}a$ ranges from $0.422c/a$ to $0.449c/a$ (pink curve in Figure 4a), not covering the whole band gap frequency range. A dipole source at the left end will excite rightward propagating waves along the flat waveguide. Within the frequency range of gapped edge states, high transmission is obtained (red curve of Figure 4b). To test the robustness of these gapped edge states, a rectangular obstacle with the size of $2a \times 2\sqrt{3}a$ is inserted as a defect. The transmission of this blocked waveguide is also recorded (black curve in Figure 4b). At most of the frequencies, the transmission of blocked waveguide is the same as that of flat waveguide. For example, E_z fields of transmitted EM waves at the frequency of $0.44c/a$ can wrap around the inserting obstacle and keep moving rightward, demonstrating the robustness of gapped edge states (right panel of Figure 4c). At some other frequencies, the transmission of block waveguide drops little but still keeps high value, indicating the high transmission of gapped edge states (Figure 4d). Note that the frequency range of gapped edge states can be changed

for boundary terminations with different τ , showing a potential application in bandwidth-controllable robust waveguide.

Robustness or high transmission against obstacles is not always true for all gapped edge states. Figure 5 illustrates a comparative example showing that such predominant property is protected by the nontrivial topology of band gap, instead of the nonzero bianisotropy. The comparative PC consists of air rods ($r = 0.46a$) in the dielectric background with $\varepsilon_r = 15$. The bianisotropic coefficient is kept unchanged as $\zeta_0 = 0.9$, being the same as that of PC in Figure 3f. When increasing ζ_0 from 0 to 0.9, no band inversion is observed and thus the band gap is topologically trivial (see details in Supporting Information D). For a fair comparison, the width of band gap (highlighted in green) is tuned to be the same as that of the nontrivial PC in Figure 2f. Figure 5b shows the gapped edge states when the bulk PC is terminated with a trivial homogeneous insulator. The edge termination parameter is chosen to be $\tau = 0.24\sqrt{3}a$ to have edge dispersions ranging from $0.422c/a$ to $0.449c/a$, being similar to that in Figure 4a. Figure 5c illustrates that the transmission of blocked waveguide (black) is several orders of magnitude less than that of flat waveguide (red) in the whole frequency range of gapped edge states. In contrast to the high transmission of gapped edge states in topological PCs, the EM waves experience strong backscattering. The inserting obstacle will totally block the rightward propagating waves and it leads to no output energy at the right exit (Figure 5d).

3. Conclusion

In conclusion, we show that accidental double Dirac cones can be restored in non-magnetic PCs with anisotropic permittivity by achieving degeneracy between TE and TM modes. We deduce the simplified gap opening condition based on group symmetry analysis, and demonstrate that the realization of double Dirac cones is not the sufficient condition to open the band gap. Topological anisotropic PCs are obtained by breaking nontrivial double Dirac cones, each of which is formed by TE and TM modes with the same mirror parity. Gapless edge states and their robustness against bends with different turning angles are demonstrated at the domain wall between two topologically distinct anisotropic PCs. We also show the high transmission of gapped edge states in topological anisotropic PCs, showing as a comparison to the strongly backscattered gapped edge states in trivial PCs. In Supporting Information E, we give an experimental design of the proposed anisotropic PCs.

Supporting Information

Supporting Information is available from the Wiley Online Library or from the author.

Acknowledgements

This work was supported by National Natural Science Foundation of China (11522437, 11704422, 61775243, 11761161002), and Fundamental Research Funds for the Central Universities (No.17lgpy19).

Conflict of Interest

The authors declare no conflict of interest.

Keywords

anisotropy, Dirac cones, photonic crystals, topological photonics

Received: March 13, 2018

Revised: August 20, 2018

Published online:

- [1] K. Xie, H. Jiang, A. D. Boardman, Y. Liu, Z. Wu, M. Xie, P. Jiang, Q. Xu, M. Yu, L. E. Davis, *Laser Photonics Rev.* **2014**, *8*, 583.
- [2] Z. Yang, F. Gao, X. Shi, X. Lin, Z. Gao, Y. Chong, B. Zhang, *Phys. Rev. Lett.* **2015**, *114*, 114301.
- [3] M. Hasan, C. Kane, *Rev. Mod. Phys.* **2010**, *82*, 3045.
- [4] E. Goi, Z. J. Yue, B. P. Cumming, M. Gu, *Laser Photonics Rev.* **2018**, *12*, 1700271.
- [5] L. Xia, W. Gao, B. Yang, Q. Guo, H. Liu, J. Han, W. Zhang, S. Zhang, *Laser Photonics Rev.* **2018**, *12*, 1700226.
- [6] M. Xiao, W. Chen, W. He, C. T. Chan, *Nat. Phys.* **2015**, *11*, 920.
- [7] X. Wan, A. M. Turner, A. Vishwanath, S. Y. Savrasov, *Phys. Rev. B* **2011**, *83*, 205101.
- [8] X. Huang, Y. Lai, Z. H. Hang, H. Zheng, C. T. Chan, *Nat. Mater.* **2011**, *10*, 582.
- [9] C. T. Chan, Z. H. Hang, X. Huang, *Adv. Optoelectron.* **2012**, *2012*, 1.
- [10] J.-W. Dong, M.-L. Chang, X.-Q. Huang, Z. H. Hang, Z.-C. Zhong, W.-J. Chen, Z.-Y. Huang, C. T. Chan, *Phys. Rev. Lett.* **2015**, *114*, 163901.
- [11] Y. Fu, L. Xu, Z. H. Hang, H. Chen, *Appl. Phys. Lett.* **2014**, *104*, 193509.
- [12] P. Moitra, Y. Yang, Z. Anderson, I. I. Kravchenko, D. P. Briggs, J. Valentine, *Nat. Photonics* **2013**, *7*, 791.
- [13] Y. Li, S. Kita, P. Muñoz, O. Reshef, D. I. Vulis, M. Yin, M. Lončar, E. Mazur, *Nat. Photonics* **2015**, *9*, 738.
- [14] L.-H. Wu, X. Hu, *Phys. Rev. Lett.* **2015**, *114*, 223901.
- [15] C. He, X. Ni, H. Ge, X.-C. Sun, Y.-B. Chen, M.-H. Lu, X.-P. Liu, Y.-F. Chen, *Nat. Phys.* **2016**, *12*, 1124.
- [16] Z.-G. Chen, J. Mei, X.-C. Sun, X. Zhang, J. Zhao, Y. Wu, *Phys. Rev. A* **2017**, *95*, 043827.
- [17] B.-Z. Xia, T.-T. Liu, G.-L. Huang, H.-Q. Dai, J.-R. Jiao, X.-G. Zang, D.-J. Yu, S.-J. Zheng, J. Liu, *Phys. Rev. B* **2017**, *96*, 094106.
- [18] F. Haldane, S. Raghu, *Phys. Rev. Lett.* **2008**, *100*, 013904.
- [19] X. Ao, Z. Lin, C. Chan, *Phys. Rev. B* **2009**, *80*, 033105.
- [20] A. B. Khanikaev, S. H. Mousavi, W.-K. Tse, M. Kargarian, A. H. MacDonald, G. Shvets, *Nat. Mater.* **2013**, *12*, 233.
- [21] T. Ma, G. Shvets, *Phys. Rev. B* **2017**, *95*, 165102.
- [22] M. C. Rechtsman, J. M. Zeuner, Y. Plotnik, Y. Lumer, D. Podolsky, F. Dreisow, S. Nolte, M. Segev, A. Szameit, *Nature* **2013**, *496*, 196.
- [23] X.-D. Chen, F.-L. Zhao, M. Chen, J.-W. Dong, *Phys. Rev. B* **2017**, *96*, 020202(R).
- [24] X.-L. Qi, S.-C. Zhang, *Rev. Mod. Phys.* **2011**, *83*, 1057.
- [25] A. B. Khanikaev, R. Fleury, S. H. Mousavi, A. Alu, *Nat. Commun.* **2015**, *6*, 8260.
- [26] L. Lu, J. D. Joannopoulos, M. Soljačić, *Nat. Photonics* **2014**, *8*, 821.
- [27] Y. Wu, C. Li, X. Hu, Y. Ao, Y. Zhao, Q. Gong, *Adv. Opt. Mater.* **2017**, *5*, 1700357.
- [28] C. He, L. Lin, X.-C. Sun, X.-P. Liu, M.-H. Lu, Y.-F. Chen, *Int. J. Mod. Phys. B* **2014**, *28*, 1441001.
- [29] M. G. Silveirinha, *Phys. Rev. B* **2015**, *92*, 125153.
- [30] M. G. Silveirinha, *Phys. Rev. B* **2017**, *95*, 035153.
- [31] J.-W. Dong, X.-D. Chen, H. Zhu, Y. Wang, X. Zhang, *Nat. Mater.* **2017**, *16*, 298.

- [32] D. Bohm, *Quantum Theory*, Prentice-Hall Press, New York 1951.
- [33] K. Sakoda, *Optical Properties of Photonic Crystals*, Springer Science+Business Media, New York 2005.
- [34] T. Ma, A. B. Khanikaev, S. H. Mousavi, G. Shvets, *Phys Rev Lett.* **2015**, *114*, 127401.
- [35] X. Cheng, C. Jouvaud, X. Ni, S. H. Mousavi, A. Z. Genack, A. B. Khanikaev, *Nat. Mater.* **2016**, *15*, 542.
- [36] J. D. Joannopoulos, S. G. Johnson, J. N. Winn, R. D. Meade, *Photonic Crystals: Molding the Flow of Light*, Princeton University Press, Princeton, NJ 2008.
- [37] I. V. Lindell, A. H. Sihvola, *J. Electromagn. Wave* **2005**, *19*, 861.
- [38] H. M. El-Maghrabi, A. M. Attiya, E. A. Hashish. *Prog. Electromagn. Res. M* **2011**, *16*, 159.